Available online at www.sciencedirect.com

ScienceDirect

Procedia Engineering 2 (2010) 2297–2305

Procedia Engineering

www.elsevier.com/locate/procedia

Fatigue 2010

Influence of niobium alloying on the low cycle fatigue of cast TiAl alloys at room and high temperatures

T. Kruml[a], M. Petrenec[a]*, K. Obrtlík[a], J. Polák[a], P. Buček[a,b]

[a]Institute of Physics of Materials of the Academy of Sciences of the Czech Republic, Žižkova 22, Brno 616 62, Czech Republic
[b]Faculty of Mechanical Engineering, Institute of Materials Science and Engineering, Brno University of Technology, Technická 2, 616 69 Brno, Czech Republic

Received 8 March 2010; revised 12 March 2010; accepted 15 March 2010

Abstract

The low-cycle fatigue properties of TiAl alloys with 2 at.% and 7 at.% of Nb with nearly lamellar microstructure were studied at room temperature and 750°C. Cyclic hardening/softening curves, cyclic stress-strain curves (CSSC) and fatigue life curves were obtained at both temperatures as well as monotonic tensile properties. Both materials show stable cyclic response at 750°C. At room temperature, significant cyclic hardening characteristic for 2 at.%Nb alloy is not observed for 7 at.% Nb alloy. This difference is attributed to higher Nb content which increases the stacking fault energy and thus prevents intensive twinning. Parameters of the CSSC, the Manson-Coffin law and the Basquin law were determined. The cyclic strength of the alloy with 7 at.% Nb is substantially higher in comparison with 2 at.% Nb, probably due to lower thickness of the lamellas.

Keywords: Low cycle fatigue; lamellar TiAl alloy; high temperature; fracture surface.

1. Introduction

TiAl alloys are a serious candidate material for applications demanding low density, good corrosion resistance and high strength at elevated temperatures. Recently, applications using TiAl alloys appeared as e.g. parts of vehicle's engines or in aeronautics. As an example, the turbine wheel in car turbochargers is forced to rotate by exhaustion gasses at very high temperature. The material is thus subjected to centrifugal forces and temperature gradients in corrosion atmosphere; TiAl alloys are suitable materials for these conditions. Nevertheless, restricted machinability and low fracture toughness especially at room temperature represent main limitations of this material. It is hoped to improve especially the fracture properties at room temperature by increasing the Nb content to 7-8 at. %. This new generation of TiAl alloys is now under testing. In the most foreseen application, the low-cycle and/or high cycle fatigue is important, as well as the crack growth resistance of the material [1]. Studies of the low cycle fatigue properties of the high Nb TiAl alloys are rare. The first results, fatigue hardening/softening curves and fatigue life curves, are reported by Heckle and Christ [2]. Christ et al. [2,3] observed stable cyclic behaviour,

* Corresponding author. Tel.: +42-053-229-0338; fax: +42-054-121-2301
E-mail address: petrenec@ipm.cz

doi:10.1016/j.proeng.2010.03.246

satisfactory strength and lifetime at high temperatures and environmental surface embitterment which increases with temperature.

Some low cycle fatigue data measured on high Nb alloy have been already published. Room temperature and 750 °C fatigue parameters were evaluated [4], compared with the literature and complemented with fracture surface description [5] and TEM identification of most easy deformation mechanisms [6]. In this paper, new data measured on 2 at.% Nb alloy are presented, additional information about the 7 at.% Nb alloy are obtained and the performance of both materials is compared

2. Experimental procedure

2.1. Materials: chemical composition and tensile properties

The first material, TiAl with 2 at.%Nb (2Nb alloy in the following) was prepared by casting in the GfE Metalle und Materialien GmbH company in Nümberg in the form of a cylindrical ingot of 220 mm in length and 90 mm in diameter. The ingot was subjected to hot isostatic pressing (HIP) at 1280 °C and 140 MPa for 4 hours. The chemical composition of the alloy is given in Table 1. The composition does not vary considerably within the ingot. On the contrary, metallographic cross-sections studied by light and SEM microscopy showed that the microstructure at the centre differs from that at the ingot borders. Therefore, the cylindrical fatigue specimens were prepared only from the outer regions of the ingot. Micrographs of the polished and etched cross-section of the ingots are shown in Fig. 1. Figure 1a, taken from the outer part of the ingot, shows variable grains size in range from 0.08 to 1 mm. In Fig. 1c on the grain boundaries, some smaller areas without the lamellar substructure of single γ phase are present. The surface fraction of these areas is 6 %. Inside the other grains, a fine lamellar structure of γ and α_2 phases alternates, as shown in Fig. 2a. The thickness of the γ phase lamellas is about 1.95 μm.

The second material is TiAl with 7.8 at.%Nb (7Nb alloy in the following) in the form of a cylindrical ingot of 1070 mm in length and 70 mm in diameter. It was prepared by casting in the Flowserve company. The chemical composition of the alloy is shown in Table 1. As in the case of the 2Nb alloy, its composition does not vary within the ingot and the microstructure at the center differs from the ingot borders. Therefore, the cylindrical fatigue specimens were prepared only from the outer regions of the ingot. Figure 1b documents the grains of 0.1 to 1.2 mm in diameter. The fraction of single γ phase islands is about 3 %, the rest of the volume contains lamellar substructure. Fine lamellar structure of γ and α_2 phases is shown in Fig. 2b. The γ phase lamellas have average thickness of 0.87 μm. Using neutron diffraction other minority phases were identified. Their volume fraction derived from the neutron diffraction analysis is: β phase 2.8 %, β_2 phase 1.4 % and B2 phase 3.5 %. These minor phases were observed either in regions between lamellas γ and α_2 phases (see Fig. 2c) or in regions close to grain boundaries.

The nearly lamellar microstructure of both materials is thus similar. The main difference consists in different thickness of γ lamellas.

The monotonic tensile properties of studied TiAl alloys at both temperatures are presented in Table 2. At room temperature (RT), tensile tests up to the fracture were conducted. At 750 °C, tensile properties were determined from the first quarter cycle during cyclic test. The results show that both materials are rather brittle at room temperature. The comparison of both materials shows that:

- The fracture plastic strain ε_{pF} at room temperature is higher for the 7Nb alloy but still not reaching 0.2%. Therefore, only the yield stress at 0.1% of plastic strain $\sigma_{0.1}$ can be determined.
- The yield stress defined by this way is higher by 35% for the 7Nb alloy at RT and by 25% at 750 °C.
- The fracture stress at room temperature is also higher by about 180 MPa for the 7Nb alloy due to both higher strength and higher fracture plastic strain.
- The Young modulus is lower for the 7Nb alloy at both temperatures. It decreases with temperature, the difference between RT and 750 °C is 11% for the 2Nb alloy and 15% for the 7Nb alloy.

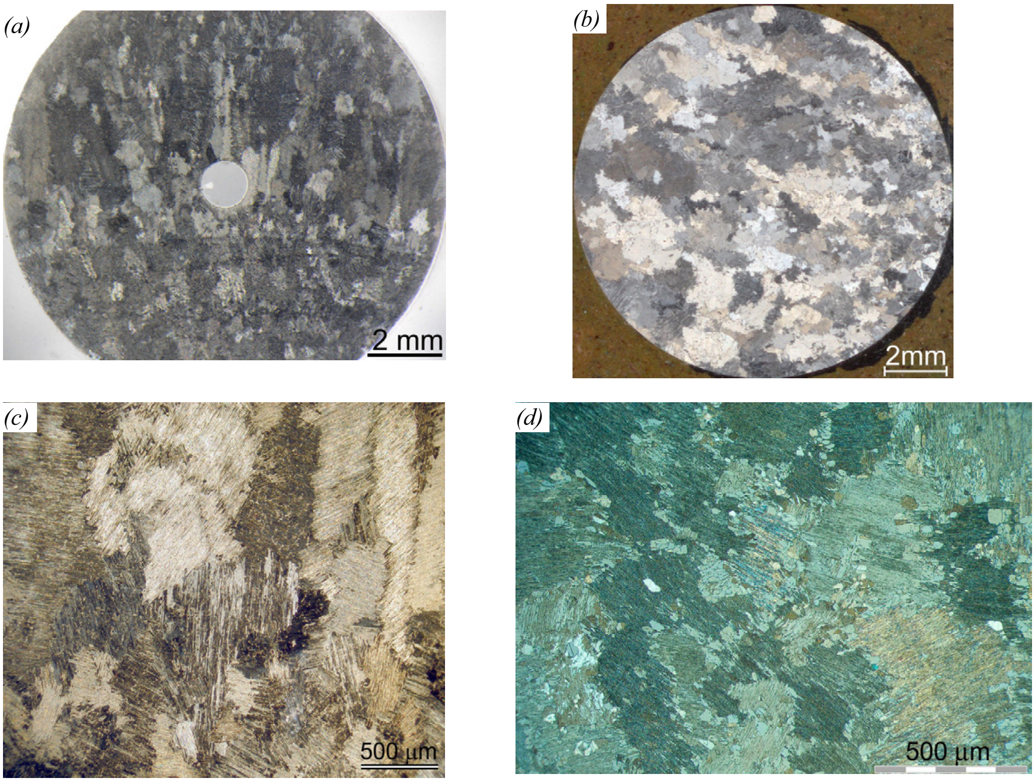

Fig. 1. Optical micrographs of the cast TiAl alloys: the head of a specimen, etched to reveal the heterogenous grain size in a section perpendicular to the ingot axis (a) 2Nb alloy and (b) 7Nb alloy; detail of central part of a specimen heads of (c) 2Nb alloy and (d) 7Nb alloy.

Table 1. Chemical composition of cast TiAl alloys (in at. %).

	Ti	Al	Nb	Cr	Ni	Si	B
2Nb alloy	47.61	47.56	2.04	1.96	–	–	0.82
7Nb alloy	47.8	44.2	7.8	0.7	0.2	0.1	–

Table 2. Tensile properties of cast TiAl alloys at two temperatures.

Temperature [°C]	material	E [GPa]	0.1 % yield stress [MPa]	fracture stress [MPa]	fracture ε_p [%]	fracture ε [%]
23	2Nb	180 ± 2	398	415	0.13	0.364
	7Nb	161 ± 2	548	593	0.18	0.545
750	2Nb	161 ± 3	357	–	–	–
	7Nb	137 ± 1	449	–	–	–

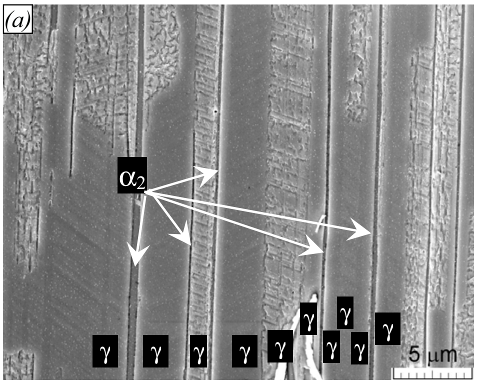

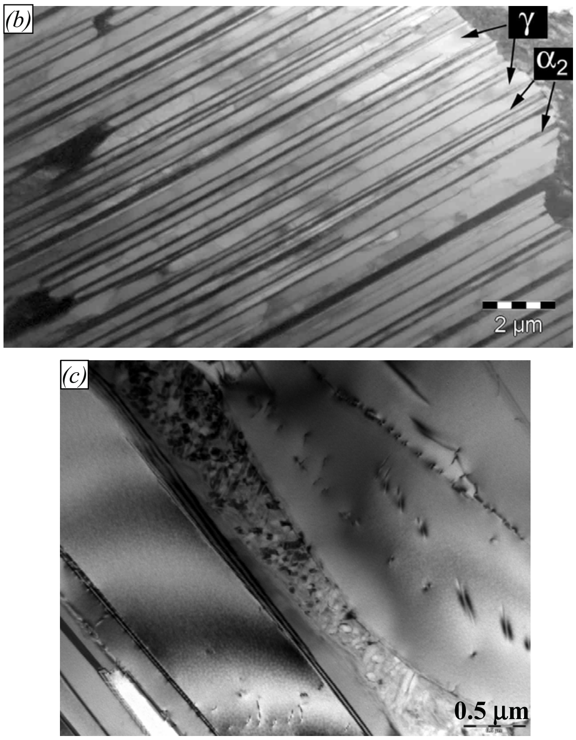

Fig. 2. Electron micrographs of lamellar microstructures of the TiAl alloys: (a) SEM image of the 2Nb alloy; (b) TEM image of the 7Nb alloy; (c) detail of a region with minor phases in the form of small spherical precipitates.

2.2. Low cycle fatigue tests

Schemes of two types of cylindrical specimens used for fatigue tests are shown in Fig. 3. It was possible to prepare the specimens by standard machining operation as turning, grinding and drilling. The gauge length was carefully mechanically and then electrolytically polished. Fatigue tests were performed under strain control using MTS servohydraulic machines in symmetric tension-compression cycle (R_ε = -1). The total strain amplitude (ε_a) and strain rate of 2×10^{-3} s^{-1} were kept constant in all tests. Strain was measured by extensometers attached directly to the gauge part of the specimens at both temperatures. The tests were performed at room temperature (RT) and 750 °C in air. Heating was provided by a three-zone resistant furnace and monitored by three thermocouples attached to both ends and to the upper part of the gauge section. During cyclic loading, hysteresis loops of selected cycles were recorded for further analysis. The stress amplitude, mean stress, total strain amplitude, Young's modulus measured from both hysteresis half-loops, maximum and minimum stress and strain were recorded for every cycle. After the test termination, a special program was used to evaluate the plastic strain amplitude (ε_{ap}) as the half-width of the hysteresis loop. The cumulative plastic strain was calculated according Eq. (1),

$$\varepsilon_c = \sum_{i=1}^{2N} \left| 2\varepsilon_{ap} \right|_i , \qquad (1)$$

where N is number of cycles.

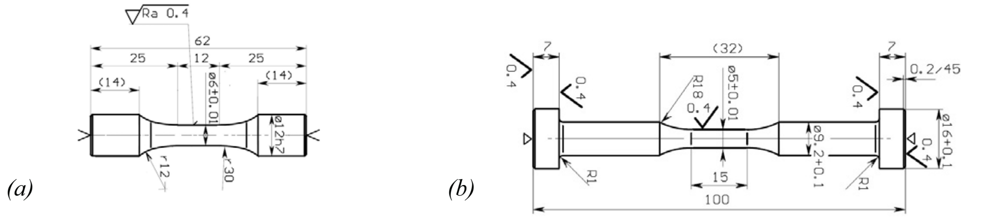

Fig. 3. Shape and dimensions of specimen in mm for low-cycle fatigue tests (a) at room temperature; (b) at high temperatures.

3. Results

3.1. Cyclic hardening-softening curves

Cyclic hardening/softening curves are presented in Fig. 4 for both temperatures and materials. These curves shows stress amplitude σ_a vs. cumulative plastic strain ε_c for tests performed with constant total strain amplitudes ε_a. The character of these curves varies with temperature and the type of TiAl alloy. Stable cyclic response is observed for the 7Nb alloy at both temperatures and also for the 2Nb alloy at 750 °C. Usually, slight cyclic softening is observed during the first 10 cycles; the stress amplitude changes no more than 5 MPa; the cyclic response is thus stable within 1% of σ_a. On the contrary, significant cyclic hardening up to fracture is observed for the 2Nb alloy at room temperature. The initial cyclic hardening is more pronounced with increasing strain amplitude. At $\varepsilon_a = 0.35\%$, the material cyclically hardens by 70 MPa during its lifetime.

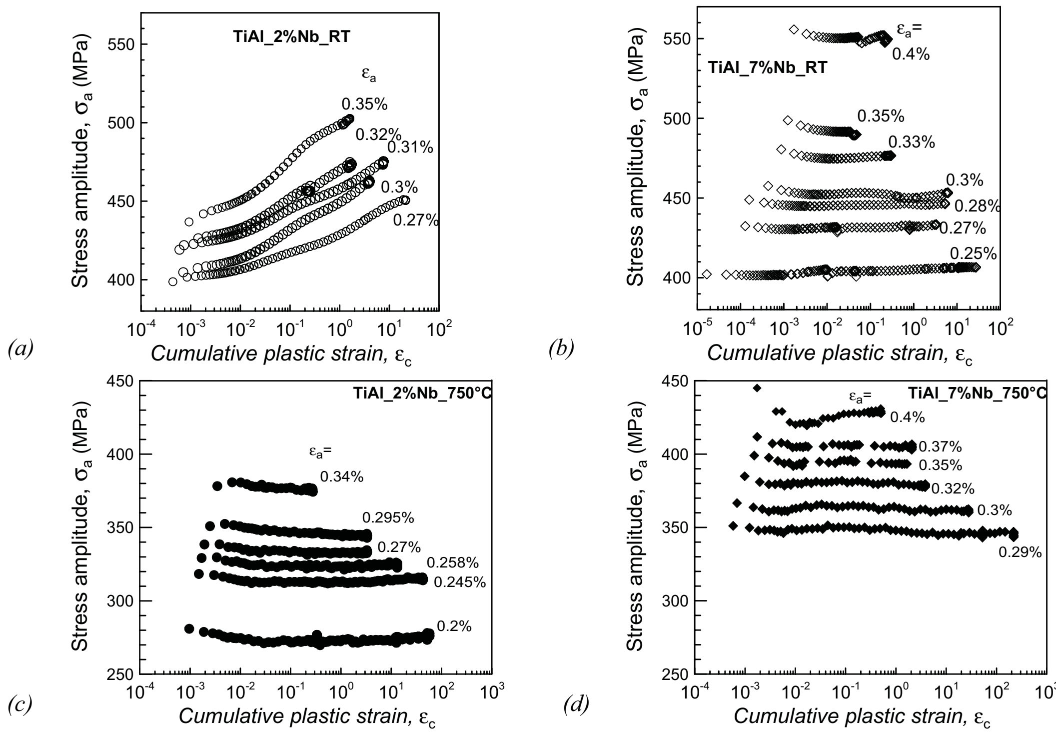

Fig. 4. Selected cyclic hardening/softening curves of both TiAl alloys in representation of σ_a vs. cumulative plastic strain ε_c. (a) 2Nb alloy, RT; (b) 7Nb alloy, RT; (c) 2Nb alloy, 750 °C (d) 7Nb alloy, 750 °C.

3.2. Cyclic stress-strain curves

The cyclic stress-strain curves (CSSCs) of TiAl alloys at both temperatures are shown in Fig. 5a. Stress amplitude σ_a is plotted vs. plastic strain amplitude ε_{ap}. Both values were taken at half life with the exception of the 2Nb alloy data at RT. The continuous hardening of the 2Nb alloy at RT makes difficulties in choosing characteristic σ_a and ε_{ap} for constant ε_a level. The scatter of number of cycles to failure N_f implies also the scatter in the half-life values of σ_a and ε_{ap}. Therefore, two values of cumulative plastic deformation ε_c were chosen and characteristic σ_a and ε_{ap} were taken at these levels. With increasing ε_c the CSSC of the 2Nb alloy at RT is shifted to higher stresses. For ε_c values higher than about 4 the subsequent changes of σ_a and ε_{ap} are small. The very good high-temperature mechanical resistance of the 7Nb alloy is documented by the CSSC at 750°C with stress amplitudes around 400 MPa. CSSCs for both materials at 750 °C have approximately the same slope and are shifted to each other of about 70 MPa. The CSSCs were approximated by the power law:

$$\sigma_a = K' \varepsilon_{ap}^{n'} \tag{2}$$

where K' is fatigue hardening coefficient and n' is fatigue hardening exponent. These material parameters were evaluated by linear regression analysis and their values are listed in Table 3.

3.3. Fatigue life curves

3.3.1. The Basquin law

The derived Wöhler curves, i.e. the relation between stress amplitude σ_a at half life or at a given cumulative plastic strain vs. number of cycles to fracture N_f are shown for both temperatures and both TiAl alloys in Fig. 5b. Moreover, data published in [7] for a TiAl lamellar alloy with 2 at.% Nb are added for comparison. Experimental data were approximated by the Basquin equation:

$$\sigma_a = \sigma_f' \left(2N_f\right)^b, \tag{3}$$

where σ_f' is fatigue strength coefficient and b is fatigue strength exponent. All material parameters were evaluated by linear regression analysis and their values are given in Table 3.

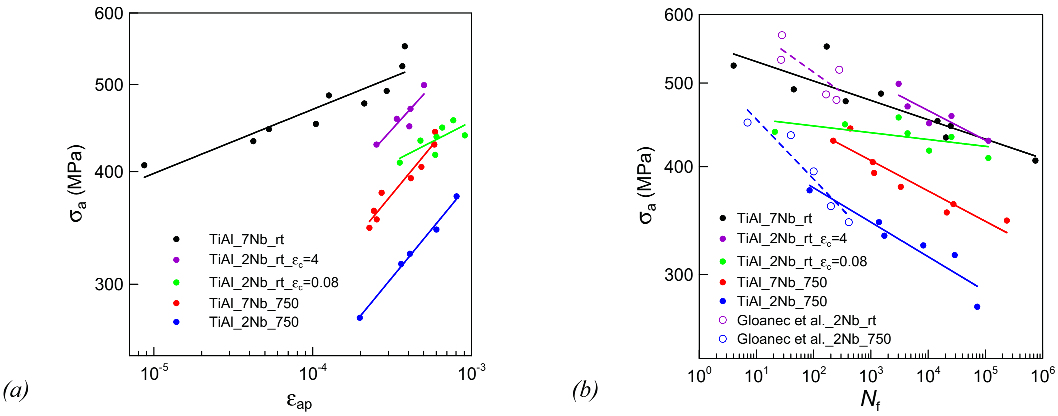

Fig. 5. The cyclic stress-strain curves (a) and the derived Wöhler curves (b) of TiAl alloys at two temperatures. Open symbols were measured earlier [7] for the 2Nb alloy.

Inspection of Fig. 5b and also of the parameters in Table 3 reveals that at room temperature these fatigue life curves of both TiAl and also of the material tested earlier [7] are quite similar within the experimental scatter. The position of the curve for 2Nb is influenced by the criterion for the choice of σ_a. For $\varepsilon_c = 4$, the data corresponds well to those published earlier [7]. Increase of the testing temperature to 750 °C decreases the strength of the materials which is reflected by the shift of Basquin curves to lower N_f as compared with RT curves.

At 750 °C, the slopes of the derived Wöhler curves and consequently the fatigue strength exponents b of 7Nb alloy and 2Nb alloy very similar. The curve for the 7Nb alloy is shifted towards longer fatigue lives; for the cycling at the same stress amplitudes, the fatigue life of the 7Nb alloy is about 2 orders of magnitude longer than for the 2Nb alloy. Data taken from [7] agree well with the data measured here for the 2Nb alloy but the slope of the curve is higher.

3.3.2. The Manson-Coffin law

In Fig. 6a plastic strain amplitude ε_{ap} vs. N_f is plotted in bilogarithmic representation. The values of ε_{ap} were chosen similarly as in the construction of CSSC. Experimental data were fitted by the Manson-Coffin law:

$$\varepsilon_{ap} = \varepsilon_f'\left(2N_f\right)^c, \tag{4}$$

where ε_f' is fatigue ductility coefficient and c is fatigue ductility exponent. Their values obtained are presented in Table 3. The RT fatigue is characterized by significant scatter of experimental data, which reflects low ductility and thus high sensitivity to the random presence of material defects.

At RT, the resistance of the 7Nb alloy to cyclic plastic straining is significantly lower in comparison with the 2Nb alloy. At 750 °C, fatigue lifetimes and fatigue ductility exponents of both materials are comparable within the experimental scatter.

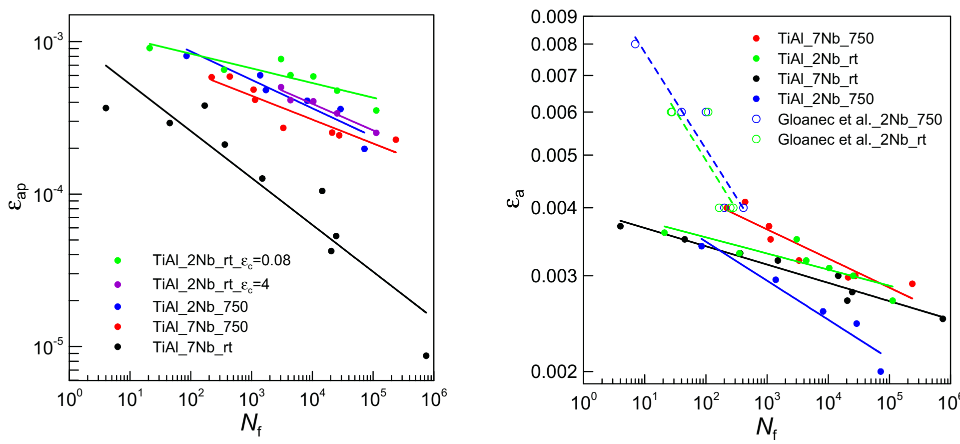

Fig. 6. Fatigue life curves of TiAl alloys at two temperatures: (a) experimental data were fitted with the Manson-Coffin law; (b) experimental data were fitted with the Basquin law.

3.3.3. Combined curve

The combined fatigue life curve is represented by the plot of ε_a vs. N_f (Fig. 6b). Mathematically, it can be composed from Basquin and Manson-Coffin laws. If the strain amplitude is decomposed into elastic and plastic components as

$$\varepsilon_a = \varepsilon_{ae} + \varepsilon_{ap} = \sigma_a/E + \varepsilon_{ap} \,, \tag{5}$$

than using eqs. (3) and (4) it may be combined into

$$\varepsilon_a = \frac{1}{E}\,\sigma'_f\,(2N_f)^b + \varepsilon'_f\,(2N_f)^c. \tag{6}$$

This is the basic fatigue life curve in this work because ε_a was kept constant during fatigue experiments. The numbers of cycles to failure for the two materials at RT are very close. At 750 °C, 7Nb alloy has higher N_f at the same ε_a in comparison with 2Nb alloy.

Table 3. Parameters of cyclic plasticity and low cycle fatigue life of TiAl alloys at two temperatures.

Temperature [°C]	material	K'[MPa]	n' [-]	ε'_f [-]	c [-]	σ'_f [MPa]	b [-]
23	2Nb and $\varepsilon_c = 0.08$	848	0.090	0.00138	- 0.096	465	- 0.008
	2Nb and $\varepsilon_c = 4$	2 140	0.195	0.00219	- 0.174	653	- 0.034
	7Nb	903	0.071	0.00132	- 0.308	542	- 0.020
750	2Nb	1 712	0.214	0.00231	- 0.186	467	- 0.040
	7Nb	2 106	0.213	0.00145	- 0.157	531	- 0.035

4. Discussion

The two TiAl materials have different chemical composition, especially the Nb content. Their grain size is nearly the same. Important is the difference in lamellas thickness, the 7Nb alloy lamellar microstructure is finer.

The cyclic behavior of the 7Nb alloy and 2Nb alloy differs significantly in two points: (i) the 7 Nb alloy exhibits higher fatigue strength (σ_a for a given ε_a is higher); (ii) strong cyclic hardening of the 2Nb alloy at RT is not observed in the 7Nb alloy.

The higher strength (both monotonic and cyclic) of the 7Nb alloy can be attributed to the effect of thickness of lamellas. Finer lamellas imply more interlamellar interfaces i.e. the barriers for dislocation movement. Indeed, Umakoshi et al. [8] compared two binary TiAl alloys with different lamellar structures. They observed the difference of the yield stress of 38% between materials with the mean lamellar spacing of 1.13 and 0.75µm respectively. In the case of our materials, the difference in the lamellar spacing is even higher which can explain the difference in strength of these materials.

The cyclic hardening of the 2Nb alloy was observed also by Hénaff and Gloanec [1] and explained by intensive twinning which causes additional obstacles for mobile dislocations. Deformation twinning is caused by the movement of individual Shockley partial dislocations. This is possible only in combination of low stacking fault energy (SFE) and high stresses. The following explanation of cyclic properties of both materials thus seems probable. For 2Nb alloy at 750 °C, SFE is high enough that the twinning is not too frequent. The cyclic behavior of the material at this temperature is thus stable. SFE decreases steadily with temperature; at RT it is low enough to enable intensive twinning resulting in strong cyclic hardening. Nb addition increases the stacking fault energy and for the 7Nb alloy, SFE is high enough to prevent frequent twinning even at room temperature. The stable cyclic behavior of the 7Nb alloy is therefore a direct consequence of the Nb addition.

5. Conclusions

Results of low cycle fatigue tests at constant strain amplitude and tensile tests at RT and 750 °C lead to the following conclusions:

- The fatigue behavior of the 2Nb alloy agrees well with the literature data measured on the material with the same chemical composition and similar microstructure.
- The 7Nb alloy exhibits higher strength, both in monotonic and cyclic loading, in comparison with the 2Nb alloy at both temperatures. This is explained by the refinement of the lamellar microstructure.
- The 2Nb alloy cyclically hardens at RT probably due to intensive twinning. On the contrary, 7Nb alloy is cyclically stable at both temperatures.
- The number of cycles to failure is about two orders of magnitude higher for the 7Nb alloy in comparison with the 2Nb alloy at 750°C and is comparable at RT for both materials.
- In the Manson-Coffin plot, both alloys have the same fatigue life at 750°C while at RT the 7Nb alloy is less resistant to cyclic plastic straining.
- Parameters of the cyclic stress-strain curve, the Basquin law and the Coffin Manson law for both materials and both temperatures were evaluated.

Acknowledgements

This research was supported by the research project No. AV0Z 20410507 of the Academy of Sciences of the Czech Republic and by the grants No. 106/08/1631 and 106/07/0762 of the Czech Science Foundation. The authors are also obliged to Mr. Dluhoš for SEM observations using Tescan MIRA 3 microscope.

References

[1] Hénaff G, Gloanec A. *Intermetallics* 2005;**13**:543.
[2] Heckle TK; Christ HJ. *6th Int. Conf. on Low Cycle Fatigue*, eds. Portella PD et al., p. 579, 2008.
[3] Christ HJ, Bauer V. *6th Int. Conf. on Low Cycle Fatigue*, eds. Portella PD et al., p. 585, 2008.
[4] Kruml T, Obrtlík K, Petrenec M, Polák J. *Int. J. Mat. Res*. 2009;**100**:349-52.
[5] Kruml T, Obrtlík K, Petrenec M, Polák J. *Key Eng. Mater*. 2010;**417-418**:585-8.
[6] Kruml T, Dlouhý A, Petrenec M, Obrtlík M, Polák J. *Journal of Physics: Conference Series*, accepted, 2010.
[7] Gloanec Al, Jouiad M, Bertheau O, Grange M, Hénaff G. *Intermetallics* 2007;**15**:520.
[8] Umakoshi Y, Yasuda HY, Nakano T. *Mat. Sci. Eng. A* 1995;**192/193**:511.